Arthritis Research & Therapy

RESEARCH

Open Access

Early prediction of bone destruction in rheumatoid arthritis through machine learning analysis of plasma metabolites

Zihan Wang[1†], Tianyi Lan[1,2†], Yi Jiao[2], Xing Wang[2], Hongwei Yu[3], Qishun Geng[4], Jiahe Xu[5], Cheng Xiao[6*], Qingwen Tao[1*] and Yuan Xu[1*]

Abstract

Background To develop a predictive model for bone destruction in patients with rheumatoid arthritis (RA), based on the characteristics of plasma metabolites and common clinical indicators.

Methods The cohort comprised 60 patients with RA, with baseline metabolite features identified using the liquid chromatograph-mass spectrometer system. Radiographic outcomes were assessed using the van der Heijde-modified total Sharp score (mTSS) following a one-year follow-up period to quantify bone destruction. The longitudinal association between metabolites and radiographic progression was analyzed using several machine learning algorithms, and the significance of core metabolites was calculated. A new model incorporating metabolites and clinical indicators was created to evaluate its predictive performance for radiographic progression; the model was compared with other prediction models.

Results The median increase in mTSS was 3.50. Of the 774 detected metabolites, 77 differed between patients with different outcomes. Core metabolites identified using the Gaussian Naive Bayes algorithm included mangiferic acid, O-acetyl-L-carnitine, 5,8,11-eicosatrienoic acid, and 16-methylheptadecanoic acid. A standardized bone erosion risk score (BERS) was developed based on these core metabolite features for assessing the radiographic progression outcome. Individuals with a high BERS exhibited a lower risk of rapid radiographic progression than those with a lower score (OR = 0.01, 95% CI = 0.01–0.03, $P = 0.003$). The "China-Japan Friendship Hospital-BERS Model" (CjBM), combining BERS with clinical features (methotrexate and C-reactive protein), produced an area under the receiver operating characteristic curve of 0.800. Moreover, compared with the reported models, the CjBM showed near statistical significance in identifying rapid radiographic progression; adding BERS can improve the discrimination of the original reported model (P_{DeLong}=0.035).

†Zihan Wang and Tianyi Lan contributed equally to this work and share first authorship.

*Correspondence:
Cheng Xiao
xc2002812@126.com
Qingwen Tao
taoqg1@sina.com
Yuan Xu
xuyuan2004020@163.com

Full list of author information is available at the end of the article

Conclusions The CjBM was developed for early prediction of bone destruction in patients with RA, and the evaluation of BERS emphasizes the significance of metabolite features.

Keywords Rheumatoid arthritis, Bone destruction, Metabolite, Machine learning, Prediction model

Introduction

Rheumatoid arthritis (RA) is a chronic and progressive autoimmune disease characterized by destructive arthritis [1]. Pathological features are synovitis and pannus, typically causing cartilage and bone erosion of the joints. In advanced stages, RA can cause joint deformity and functional loss, significantly impacting the patient's quality of life [2]. Epidemiological studies show that the incidence of RA is approximately 0.46% [3]; bone destruction-related disability increases with disease progression [4]. Identifying patients at high risk for severe joint damage early is crucial for starting treatment to slow down bone erosion. Rapid bone erosion, detectable via radiological exams, is linked to poorer prognoses [5] and can affect over 50% of patients within a year of diagnosis [6]. Elevation in clinical markers, such as C-reactive protein (CRP) and rheumatoid factor (RF), can help predict bone erosion progression in patients with RA [7], and a series of predictive models have been established [8–10]. However, the sensitivity and specificity of these markers are often limited, particularly in serologically negative patients or those receiving pharmacotherapy. Some novel biomarkers are needed to better assess disease conditions.

Several key metabolites, including lipids, glucose, and amino acids, contribute to disease diagnosis or subtyping [11]. Advanced techniques have enabled the steady identification of bioactive metabolites, offering a new field of metabolomics that may be more directly linked to certain clinical phenotypes [12]. Although some studies have focused on using metabolites to identify RA therapy response [13] and disease staging [14], few have linked their link to bone destruction. Serum arginine-related metabolites are associated with bone loss and osteoclast production [15], supporting the hypothesis that metabolites can be used to predict radiographic progression. Metabolite features will be utilized to characterize patients with RA who are at risk of bone destruction, thereby enhancing our understanding of the potential mechanisms underlying disease progression. Furthermore, specific metabolites may emerge as novel therapeutic targets.

In this prospective cohort study with a one-year follow-up, we aimed to develop an easy-to-use model to help physicians make early judgments to predict rapid radiographic progression in patients with RA based on plasma metabolite profiles and common clinical indicators. We comprehensively analyzed metabolite expression levels in patients with different bone destruction outcomes and sought to identify and screen core metabolites closely associated with radiographic progression. Moreover, we established applicable predictive models. Several machine learning (ML) algorithms were used to optimize data processing and decision-making processes.

Methods

Study cohort

This study extracted data from a randomized controlled trial (RCT) conducted at the Department of Traditional Chinese Medicine Rheumatism at the China-Japan Friendship Hospital [16]. This RCT included 176 patients aged 18–75 years with RA recruited during 2020–2021. Patients with other rheumatological or immunological systemic diseases or severe organ damage were excluded. Moreover, patients with severe joint functional impairment (such as joint deformity or loss of mobility) due to RA were excluded. Selected patients were prohibited from using biologic agents, small molecule targeted drugs, or glucocorticoids related to RA. Of the participants, who were followed for one year, 60 were randomly selected for this study, with detailed baseline and one-year data recorded. This study was approved by the China-Japan Friendship Hospital Clinical Research Ethics Committee (2020-133-K86). All patients provided written informed consent.

Diagnosis and clinical data

The diagnosis was determined according to the 2010 RA classification criteria jointly revised by the American College of Rheumatology and the European League Against Rheumatism [17]. Baseline clinical data included demographic information, body mass index (BMI), and disease duration. Additionally, the use of conventional synthetic disease-modifying antirheumatic drugs (csDMARDs) and scores of pain visual analogue scale (VAS) and Health Assessment Questionnaire-Disability Index (HAQ-DI) were recorded. Results for other variables, including RF, anticyclic citrullinated polypeptide antibody (ACPA), CRP, erythrocyte sedimentation rate (ESR), disease activity score derivative for 28 joints (DAS28), and radiographic imaging results for both hands, were collected. All the tests were conducted at the clinical lab of the China-Japan Friendship Hospital, whereas the imaging examinations were conducted at the Radiology Department.

Radiological outcome assessment

Radiological outcomes were assessed using the van der Heijde-modified total Sharp score (mTSS) to quantify the degree of joint damage in patients with RA [18]. For the 30 joint areas, the joint space narrowing Sharp score (NSS) was assessed using a four-point scale; the erosion Sharp score (ESS) was evaluated using a five-point scale. The final score was calculated as the average of two independent radiologists' evaluations, with higher scores reflecting more severe bone destruction. The total score is calculated using the formula: mTSS = NSS + ESS.

The changes in mTSS were determined by comparing baseline and one-year follow-up radiographic imaging results ($\Delta mTSS = mTSS_{one-year} - mTSS_{baseline}$). Clinical outcomes were categorized according to the median ΔmTSS in the cohort, with greater increases in mTSS indicating rapid radiographic progression.

Plasma metabolite profiling

Our study collected plasma samples from 60 patients at baseline. All samples, collected by the liquid chromatograph-mass spectrometer (LC-MS) system according to machine instructions, were analyzed using the high-resolution tandem mass spectrometer Q-Exactive (Thermo Scientific, USA) to detect metabolites. Every 10th sample was accompanied by a quality control sample (a mixture of samples) to evaluate the stability of the LC-MS during the entire collection process. Mass spectrometry data were preprocessed using the XCMS software (Version 3.18.0, Scripps Research, USA), including peak picking, peak grouping, retention time correction, secondary peak grouping, and annotation of isotopes and adducts. Metabolites were identified using the online Kyoto Encyclopedia of Genes and Genomes (KEGG), Human Metabolome Database (HMDB) databases, and precise molecular mass data (m/z). We also used an in-house database to validate metabolite annotation. Technical details are available in Supplementary Materials 1.

Core metabolite screening

Metabolite expression levels were transformed into natural logarithms for subsequent analysis. The predictive metabolites associated with radiographic progression were identified using the least absolute shrinkage and selection operator (LASSO) regression analysis for all identified metabolites. These metabolites underwent screening using several ML algorithm models, including the eXtreme Gradient Boosting (XGBoost), Light Gradient Boosting Machine (LightGBM), Random Forest, Adaptive boosting (AdBoost), Multilayer Perceptron (MLP), support vector Machine (SVM), Gaussian Naive Bayes (GNB), Decision Tree, and Gradient Boosting Decision Tree (GBDT). These models were used to predict rapid radiographic progression. In the training process, the ten-fold crossover method was used for internal validation to alleviate overfitting and improve the reliability of the results. Once all models were trained, their performance was evaluated in the training and validation sets, and the optimal model was selected.

After determining the ML algorithm's optimal efficiency, subsequent calculations were conducted, with the importance of all input metabolites reported using the SHapley Additive exPlanations (SHAP) method [19]. Step-up forward selection combined with cross-validation was employed to determine the optimal combination of several metabolites [20]. This procedure was iteratively improved by incorporating one metabolite at a time according to a pre-established order of importance; iteration was halted when the model performance did not significantly improve. The selected metabolites, referred to as core metabolites, were then introduced into the ML model to determine their predictive potential for bone destruction. All samples were randomly divided into training and test sets in a 7:3 ratio. The training and internal validation sets were built using the same method, described previously.

The screening was mainly accomplished based on the ML methods. ML algorithms and model interpretability were implemented in the Python (Version 3.9.12, Python Software Foundation, USA) environment using XGBoost (Version 2.0.1), LightGBM (Version 3.2.1), scikit-learn (Version 1.1.3), and SHAP (Version 0.43.0).

Clinical evaluation of core metabolites

A new index bone erosion risk score (BERS) was defined according to expression levels of core metabolites after screening. BERS was calculated according to the standardization and weighting method, where the expression level of each core metabolite was standardized and weighted according to their corresponding importance. Where μ and σ represent the population mean and standard deviation, the formula for BERS calculation is:

$$BERS = \sum_{i=1}^{n} w_i \cdot \frac{x_i - \mu_i}{\sigma_i}$$

To analyze how BERS stratified bone destruction outcomes, we used several methods. Cumulative incidence curves were stratified using cohort BERS percentiles. Univariate regression was employed to calculate the odds ratios (OR) of BERS for the risk of rapid radiographic progression. Further, a trend test was conducted using the BERS quartiles, with the (P0, P25) interval serving as the reference group. The restricted cubic spline (RCS) was utilized to investigate potential linear or nonlinear associations between BERS and rapid radiographic progression. Knots were selected based on the Akaike information criterion within a range from the 3rd to the 7th

percentile, using OR = 1 at the median score as the reference [21].

Statistical analysis

Data was analyzed and visualized using IBM SPSS Statistics (Version 25.0, IBM Corp., USA) and R (Version 4.1.1, R Foundation for Statistical Computing, Austria). Descriptive statistics, including means, standard deviation, median, interquartile range, and proportions, were employed to present baseline data. Independent samples t-tests were utilized for normally distributed data, rank sum test (Wilcoxon) for non-normally distributed data, and chi-square test for count data. The Pearson correlation test was utilized to assess the relationship between two variables. This test measures the strength of the correlation (r, $-1 < r < 1$), with values closer to 0 indicating a weaker correlation.

To explore the ability of BERS to predict bone destruction, we used a logistic regression (LR) algorithm for model construction; the effect size was reported in ORs and measures of precision (95% confidence intervals [CI]). The basic model was developed based on clinical indicators alone; subsequent models combined BERS with clinical indicators. The receiver operating characteristic (ROC) curve was plotted to obtain the area under the curve (AUC) to assess the accuracy of the prediction model recognition. Curves were drawn to measure the calibration of the model. Decision curve analysis (DCA) was used to evaluate the clinical applicability of the model. The DeLong method was used to test the significance of AUC differences [22]. Net reclassification improvement (NRI) was used to compare the accuracy of different models [23]. We utilized the nomogram to explain the model and developed an online risk calculator based on interactive web applications with R/Shiny (Version 1.8.1.1) [24].

Statistical significance was set at $P < 0.05$.

Results

Baseline clinical features of the study cohort

The overall research design is shown in Fig. 1. This study enrolled 60 patients with RA who completed the follow-up. These patients underwent radiographic imaging of both hands at baseline and at one-year follow-up to evaluate the radiographic progression of bone destruction. The median mTSS for all patients at baseline was 13.50, whereas the median ΔmTSS assessed at one-year follow-up was 3.50. According to the median ΔmTSS of the study cohort, patients were categorized into two groups: "slow progression" ($\Delta mTSS \leq 3.50$) and "rapid progression" ($\Delta mTSS > 3.50$). In this study, patients categorized as having "rapid progression" were defined as those with rapid radiographic progression. All clinical features are presented in Table 1. Univariate analysis revealed a significant difference between the two groups solely in methotrexate (MTX) utilization, with the slow

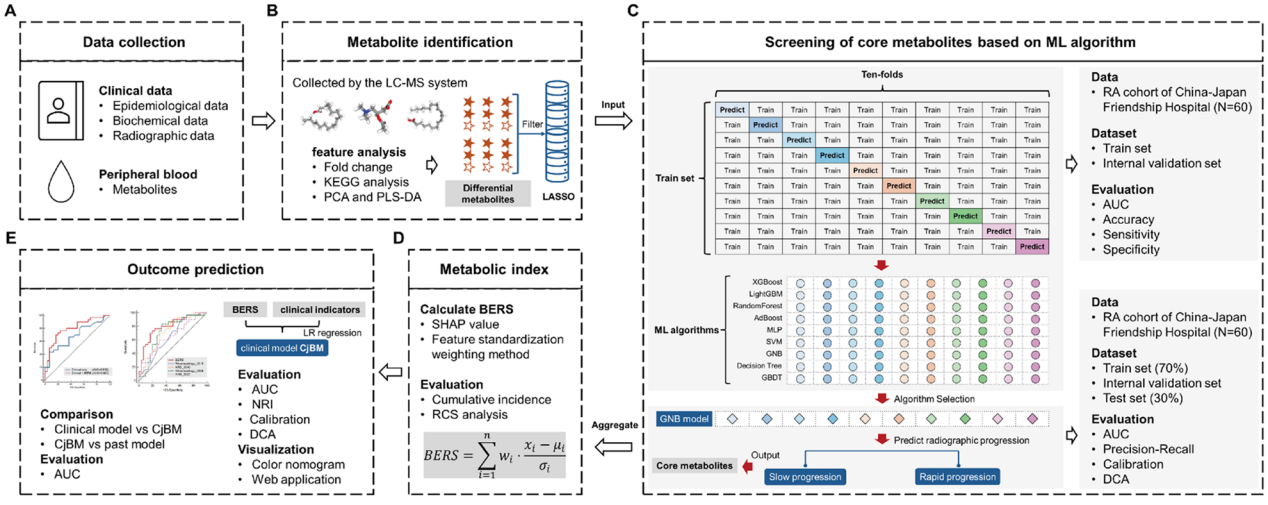

Fig. 1 Research process and design. (**A**) Clinical data and biological samples were collected from the China-Japan Friendship Hospital. (**B**) Identification, analysis, and initial screening of metabolites. (**C**) Screening of core metabolites closely related to the clinical outcomes of bone destruction is achieved through various ML algorithm models. (**D**) Calculated BERS index integrating the features of metabolites. (**E**) Model "CjBM" construction and evaluation for predicting bone destruction. Abbreviations: BERS, Bone Erosion Risk Score; CjBM, China-Japan Friendship Hospital-BERS Model; ML, machine learning; LC-MS, liquid chromatograph-mass spectrometer; KEGG, Kyoto Encyclopedia of Genes and Genomes; PCA, principal component analysis; PLS-DA, partial least squares discriminant analysis; LASSO, least absolute shrinkage and selection operator; RA, rheumatoid arthritis; AUC, area under the curve; DCA, decision curve analysis; SHAP, SHapley Additive exPlanations; RCS, restricted cubic spline; NRI, net reclassification improvement; LR, logistic regression; XGBoost, eXtreme Gradient Boosting; LightGBM, Light Gradient Boosting Machine; AdBoost, Adaptive boosting; MLP, Multilayer Perceptron; SVM, support vector Machine; GNB, Gaussian Naive Bayes; GBDT, Gradient Boosting Decision Tree

Table 1 Baseline clinical features of the study cohort

	All patients (*N* = 60)	Slow progression (*N* = 30)	Rapid progression (*N* = 30)	*P* value[a]
Age (years), mean ± SD	60.95 ± 9.32	61.13 ± 9.83	60.77 ± 8.78	0.881
Sex, female, N (%)	43 (71.7%)	22 (73.3%)	21 (70.0%)	0.774
BMI (kg/m^2), mean ± SD	22.97 ± 1.48	22.99 ± 1.53	22.96 ± 1.45	0.938
Smoking, N (%)	19 (31.7%)	7 (23.3%)	12 (40.0%)	0.165
Drinking, N (%)	21 (35.0%)	9 (30.0%)	12 (40.0%)	0.417
Duration (years), median [IQR]	7.00 [5.00]	6.50 [4.30]	7.00 [4.60]	0.297
Drugs used, N (%)				
MTX	47 (78.3%)	27 (90.0%)	20 (66.7%)	0.028
LEF	13 (21.7%)	6 (20.0%)	7 (23.3%)	0.754
IGU	13 (21.7%)	7 (23.3%)	6 (20.0%)	0.754
HCQ	35 (58.3%)	16 (53.3%)	19 (63.3%)	0.432
RF, positive, N (%)	51 (85.0%)	23 (76.7%)	28 (93.3%)	0.071
ACPA, positive, N (%)	54 (90.0%)	29 (96.7%)	25 (83.3%)	0.085
ESR (mm/h), median [IQR]	23.50 [29.00]	23.00 [33.00]	31.00 [27.00]	0.296
CRP (mg/l), median [IQR]	11.95 [17.33]	8.95 [17.40]	12.45 [14.48]	0.149
Pain VAS, median [IQR]	3.00 [1.00]	3.00 [1.00]	3.00 [2.30]	0.613
HAQ-DI, mean ± SD	0.91 ± 0.24	0.90 ± 0.24	0.91 ± 0.26	0.845
TJC28, median [IQR]	4.00 [3.0]	4.00 [3.00]	4.00 [3.00]	0.875
SJC28, median [IQR]	2.00 [4.00]	2.00 [4.25]	2.00 [3.25]	0.244
DAS28, mean ± SD	3.54 ± 0.70	3.61 ± 0.71	3.48 ± 0.70	0.448
MTSS, median [IQR]	13.50 [14.00]	12.00 [12.00]	14.00 [21.00]	0.297
ΔMTSS, median [IQR]	3.50 [4.75]	1.50 [1.00]	6.00 [4.00]	< 0.001

[a] The difference analysis between slow progression slow progression group and rapid progression group was based on independent sample test

Abbreviations: BMI, body mass index; MTX, methotrexate; LEF, leflunomide; IGU, iguratimod; HCQ, hydroxychloroquine; RF, rheumatoid factors; ACPA, anticyclic citrullinated polypeptide antibody; ESR, erythrocyte sedimentation rate; CRP, C-reactive protein; VAS, Visual Analogue Scale; HAQ-DI, Health Assessment Questionnaire-Disability Index; TJC28, tender joint counts for 28 joints; SJC28, swollen joint count for 28 joints; DAS28, Disease activity score derivative for 28 joints; NSS, narrowing Sharp score; ESS, erosion Sharp score; MTSS, van der Heijde-modified total Sharp score; $\Delta MTSS = MTSS_{one-year} - MTSS_{baseline}$

progression group exhibiting a higher frequency of MTX utilization.

Metabolite features

All patients were tested for plasma metabolites at baseline. Of 774 detected metabolites, 753 were grouped into 15 superclasses (Fig. 2A). Most metabolites belong to lipids or lipid-like molecules (450, 58.14%). KEGG analysis showed enrichment in lipid metabolism, glycan biosynthesis and metabolism, amino acid metabolism, and carbohydrate metabolism. The analysis also highlighted enrichment in cellular processes such as transport, catabolism, and cell growth and death (Fig. 2B).

Principal component analysis (PCA) was used to visualize metabolite characteristics between the groups. The slow and rapid progression groups exhibited a clear distinction in metabolite composition despite some clustering of certain samples (Fig. 2C). Partial least squares discriminant analysis (PLS-DA) yielded similar results (Figure S1). A total of 77 metabolites were significantly different between the two groups. Compared with the slow progression group, the rapid progression group exhibited increased expression of nine metabolites, whereas 68 metabolites showed decreased expression (Fig. 2D, E). The heat plot illustrates these changes (Fig. 2F). Differential metabolites are categorized into seven superclasses, with the majority classified as lipids or lipid-like molecules. The corresponding signature metabolites and their respective superclasses are illustrated in Fig. 2G.

Screening of core metabolites based on ML algorithm

To summarize the characteristics of plasma metabolites in the two groups, we aimed to identify the most critical metabolites from the total dataset. First, LASSO regression was employed for large-scale variable selection, identifying 23 metabolites from 774 (Fig. 3A, B).

Subsequent refinement was performed using various ML algorithms. The 23 metabolites were input into nine ML models (XGBoost, LightGBM, Random Forest, AdaBoost, Decision Tree, GBDT, GNB, MLP, and SVM) as independent variables. The sample outcome was then determined (slow or rapid progression group). Among these models, Random Forest showed the best performance in the training set (AUC = 1.000), whereas GNB showed the best results in the validation set (AUC = 1.000) (Table S1). Random Forest was discarded to mitigate the risk of potential overfitting, and GNB was selected for subsequent analysis due to its stability (Fig. 3C, D, Figure S2).

The importance values of 23 metabolites were calculated in the GNB algorithm using the SHAP method, with the exact values shown in the bar chart, and the optimal combination of four core metabolites was found through step-up forward selection and cross-validation (Fig. 3E). These metabolites included mangiferic acid ($r = -0.633$, $P < 0.001$), O-acetyl-L-carnitine ($r = -0.474$, $P < 0.001$), 5,8,11-eicosatrienoic acid ($r = -0.518$, $P < 0.001$), and 16-methylheptadecanoic acid ($r = -0.409$, $P = 0.001$). The levels of these four metabolites were lower in the rapid progression group compared with the slow progression group, with r-values indicating a negative correlation with rapid progression outcome. This metabolite combination was fed into the GNB algorithm model, which showed excellent differentiation of rapid radiographic progression risk outcomes in the training, validation, and test sets (Fig. 3F, Figure S3). The importance values of the

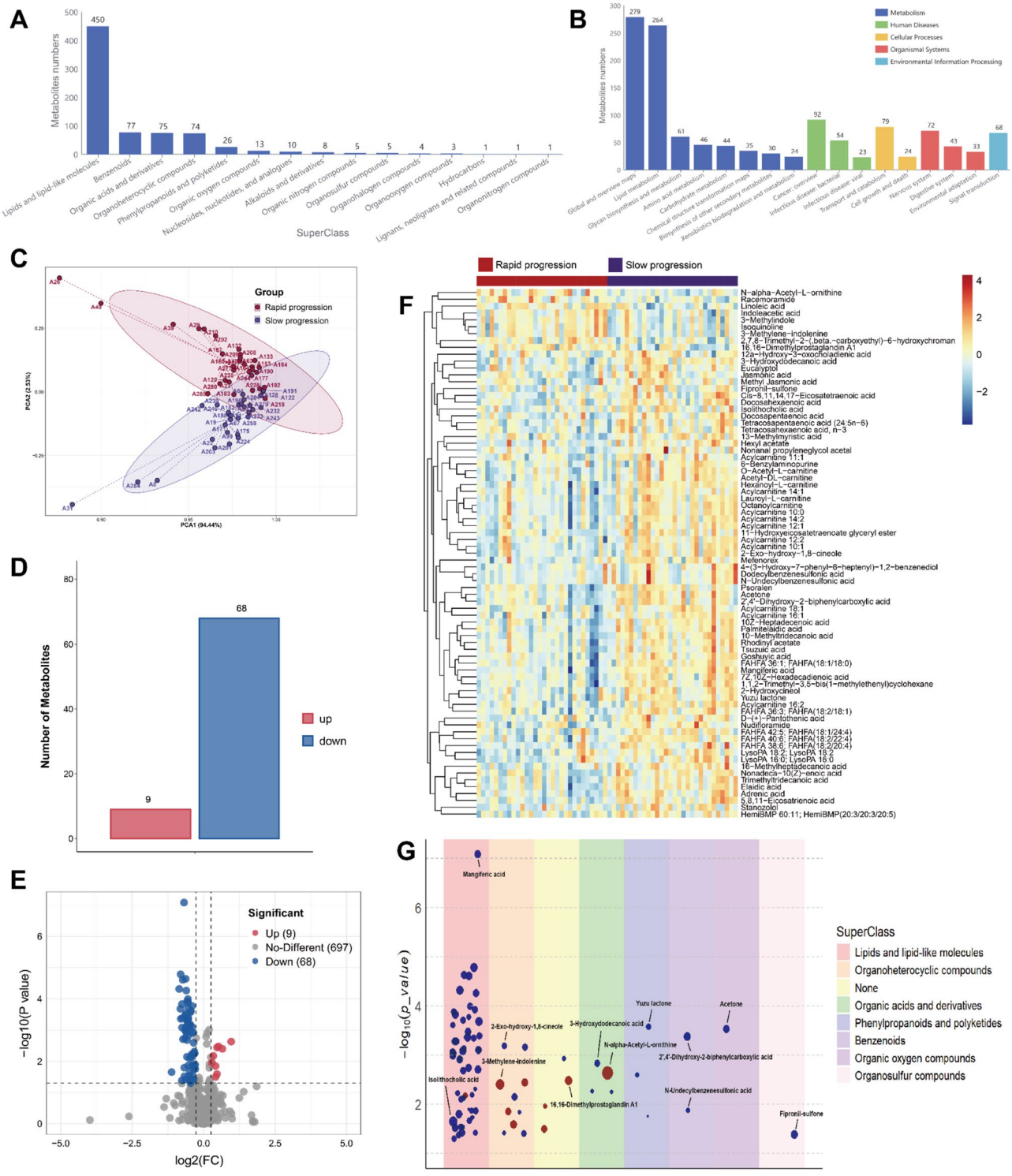

Fig. 2 Metabolite features of patients at baseline. (**A**) Identified metabolites and their respective superclasses. (**B**) KEGG analysis of metabolites. (**C**) PCA of metabolite features with different outcomes of bone destruction. (**D**) The number and trend of metabolites that differ between the two groups. The slow progression group was the reference. (**E**) Volcano plot of differential metabolites. (**F**) Heat plot of differential metabolites. (**G**) Feature plot of differential metabolites. The X-axis is classified based on the superclasses, and the Y-axis is sorted according to difference significance. Red coordinate points indicate an increase, blue ones indicate a decrease, and the size of the points is directly proportional to the multiple of change. Abbreviations: KEGG, Kyoto Encyclopedia of Genes and Genomes; PCA, principal component analysis

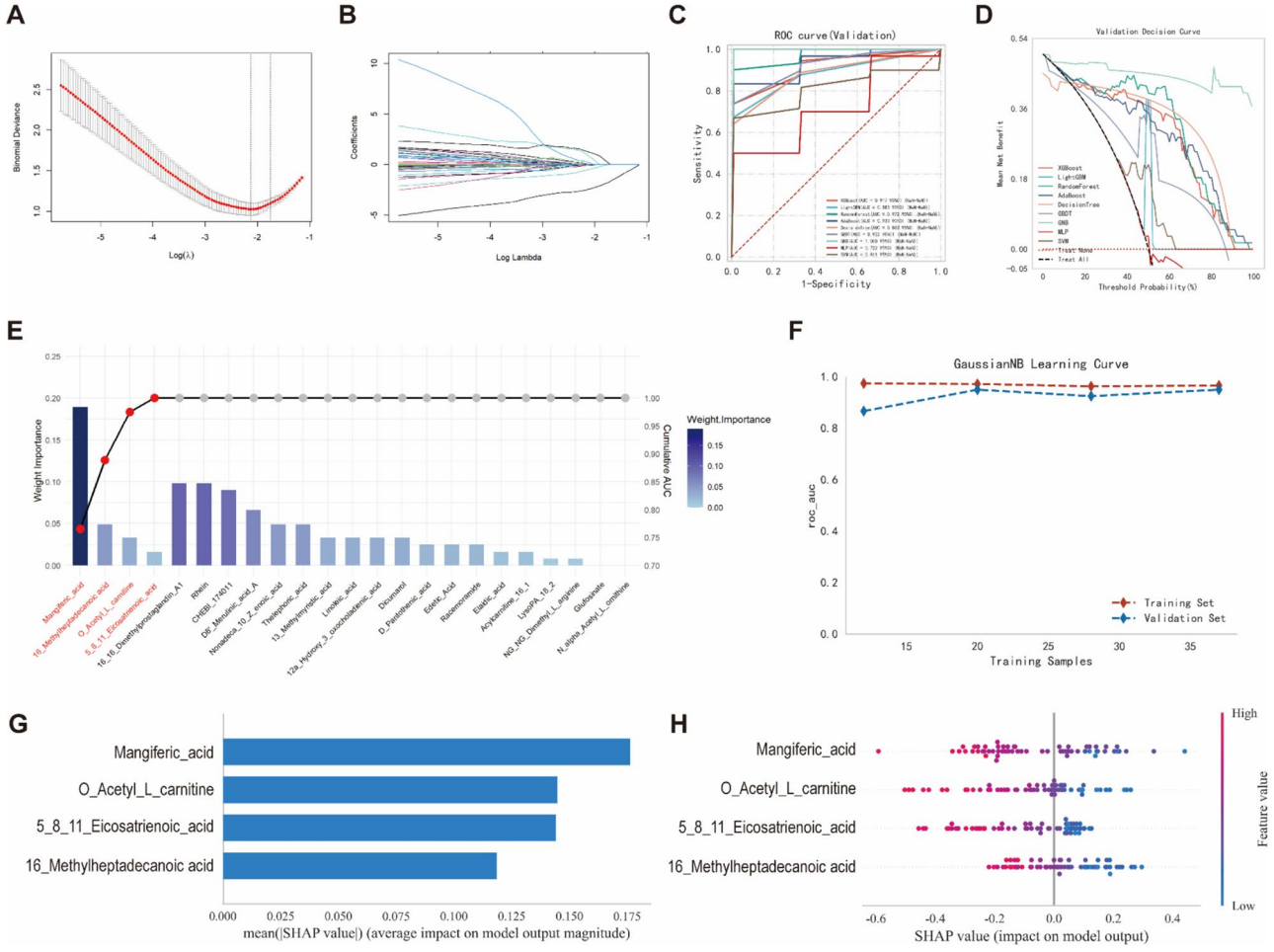

Fig. 3 Screening of core metabolites associated with the outcome of bone destruction. (**A**) LASSO regression was employed to screen for potential key metabolites. A dotted line was plotted at the lambda.min and lambda-S.E. values. The lambda.min indicates the lambda value that yields the minimum error through tenfold cross-validation; the lambda-S.E. represents one standard error to the right of lambda.min. The lambda.min was selected as the screening criterion for the final equation. (**B**) LASSO regression coefficient path plot. (**C**) ROC curves for nine ML algorithm models in the validation set. (**D**) DCA for nine ML algorithm models in the validation set. (**E**) The metabolites screened by LASSO regression were incorporated into the GNB model for further selection. The bar plot indicates the significance of the metabolites (left Y-axis). The line plot depicts the AUC values when each metabolite was included in consecutive iterations (right Y-axis). The core metabolites ultimately selected are prominently displayed in red. (**F**) Fitting of the GNB model constructed using four core metabolites during consecutive iterations. (**G**) A bar plot presenting the individual SHAP values of the four core metabolites. (**H**) The individual SHAP values of the four core metabolites are sorted according to their contributions. The X-axis indicates the magnitude of the SHAP value for each metabolite, signifying their contribution to the prediction. The color range corresponds to each metabolite value, ranging from blue (low value) to red (high value). Abbreviations: LASSO, least absolute shrinkage and selection operator; S.E., standard error; ROC, receiver operating characteristic; DCA, decision curve analysis; ML, machine learning; GNB, Gaussian Naive Bayes; AUC, area under the curve; SHAP, SHapley Additive exPlanations

four core metabolites were calculated and reported for model interpretation (Fig. 3G, H).

Metabolites correlated with the clinical outcomes of bone destruction progression

The four core metabolites were utilized to compute the overall metabolic index, referred to as the standardized BERS. The values of BERS in the two groups of patients were presented in the box plot (Fig. 4A), and the differential analysis reveals that BERS shows a higher level in the slow progression group ($P < 0.001$). We explored the link between BERS and the risk of bone destruction-related clinical outcomes. Higher BERS values correlated with a lower risk of rapid radiographic progression (Fig. 4B). Univariate regression results suggested a negative correlation between BERS and rapid radiographic progression (OR = 0.01, 95% CI = 0.01–0.03, $P = 0.003$). Trend tests detected a reduced risk among patients in the 3rd and 4th percentiles (Table 2). RCS demonstrated a nonlinear relationship between BERS and the risk of rapid radiographic progression, with a marked increase in risk as a higher BERS decreased toward the median range (Fig. 4C).

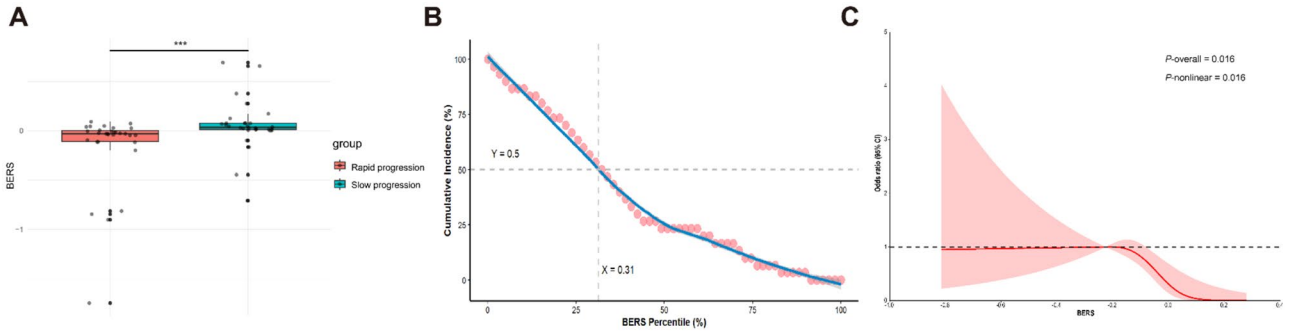

Fig. 4 BERS indicates bone destruction outcomes. (**A**) The level difference of BERS in the two groups of patients. ***$P < 0.001$. (**B**) A dot plot representing the study cohort; the BERS percentiles correlated with the observed incidence of rapid radiographic progression. (**C**) RCS analysis for modeling BERS indicates that higher BERS values are associated with a reduced risk of rapid radiographic progression. Abbreviations: BERS, Bone Erosion Risk Score; RCS, restricted cubic spline; CI, confidence intervals

Table 2 Correlation trend test of BERS and rapid radiographic progression risk

Variables	β	S.E.	OR (95%CI)	P_{trend} value
BERS standard quantile				
Q1 (<-0.446)			*Ref.*	
Q2 (-0.446, 0.008)	0.37	0.87	1.45 (0.26–8.01)	0.667
Q3 (-0.008, 0.479)	-1.70	0.80	0.18 (0.04–0.87)	0.033
Q4 (>0.479)	-2.88	0.96	0.06 (0.01–0.37)	0.003

Abbreviations: BERS, Bone Erosion Risk Score; Q1, 1st quartile; Q2, 2nd quartile; Q3, 3rd quartile; Q4, 4th quartile; β, regression coefficient; S.E., standard error; OR, odds ratio; CI, confidence intervals

Table 3 A clinical model and a combined BERS model were established based on LR algorithm

	Clinical Model[1]		Clinical + BERS Model[2]	
	OR (95% CI)	*P* value	OR (95% CI)	*P* value
MTX				
No	*Ref.*		*Ref.*	
Yes	0.209 (0.050–0.876)	0.032	0.114 (0.022–0.587)	0.009
CRP	1.044 (0.995–1.096)	0.078	0.232 (0.978–1.095)	0.232
BERS	NA		0.020 (0.001–0.616)	0.025

[1] The model was established based on clinical indicators, including MTX and CRP

[2] The model was established based on BERS, MTX and CRP

Abbreviations: BERS, Bone Erosion Risk Score; OR, odds ratio; CI, confidence intervals; MTX, methotrexate; CRP, C-reactive protein

BERS combined with clinical indicators facilitates early prediction of bone destruction

All collected clinical indicators were used to create a predictive model for bone destruction. Multi-factor LR was used as the primary algorithm for model construction. Clinical indicators such as MTX (OR = 0.209, 95% CI = 0.050–0.876, $P = 0.032$) and CRP (OR = 1.044, 95% CI = 0.995–1.096, $P = 0.078$) were included as core variables. Further, BERS (OR = 0.020, 95% CI = 0.001–0.616, $P = 0.025$) were added to construct a new prediction model (Table 3); the final model was named "China-Japan Friendship Hospital-BERS Model" (CjBM). ROC curve analysis demonstrated that BERS inclusion significantly enhanced the AUC (0.800 vs. 0.692, P_{DeLong}=0.045), indicating higher discriminatory power (Fig. 5A). The calculated NRI (0.200 ± 0.122) showed that the accuracy of the CjBM was better than that of the basic clinical model. The calibration curves and DCA indicated that the CjBM had a good calibration degree and clinical applicability (Fig. 5B, C). Specifically, CjBM demonstrated a sensitivity of 76.7%, specificity of 76.7%, positive predictive value of 81.0%, and negative predictive value of 66.7%, the detailed model parameters are provided in Table S2.

We developed a color nomogram for model visualization (Fig. 5D) and deployed an interactive web application (https://wangzihanprediction.shinyapps.io/BERS_Calculator/). When clinically applied, the CjBM can be used to predict the risk of developing rapid radiographic progression in patients with RA after a 12-month treatment by inputting identified variables. For example, an initial evaluation of a 61-year-old woman with RA who regularly took MTX showed a recent CRP of 37 mg/L. A BERS of – 0.40 showed that she had an approximately 85.7% risk of developing rapid radiographic progression after 12 months (Fig. 5E).

Moreover, four metabolites were independently evaluated to assess their predictive potential for rapid radiographic progression (Fig. 5F, Figure S4). All metabolites, except for 16-methylheptadecanoic acid (AUC = 0.793, 95% CI = 0.669–0.887, P_{DeLong}=0.077), significantly improved model performance when added individually. The largest increase was observed with mangiferic acid (AUC = 0.969, 95% CI = 0.889–0.997, P_{DeLong}=0.001). Detailed model parameters are provided in Table S3.

In this study cohort, we compared the newly established CjBM with previously reported models. The four models reported recently were directly compared [7, 9, 10, 25]. The CjBM exhibited a higher AUC value (Fig. 5G), although the difference analysis only nearly approached a statistical significance (Table S4). Furthermore, the 2019 model, which included RF, ESS, CRP, and swollen joint count for 28 joints (SJC28), was used

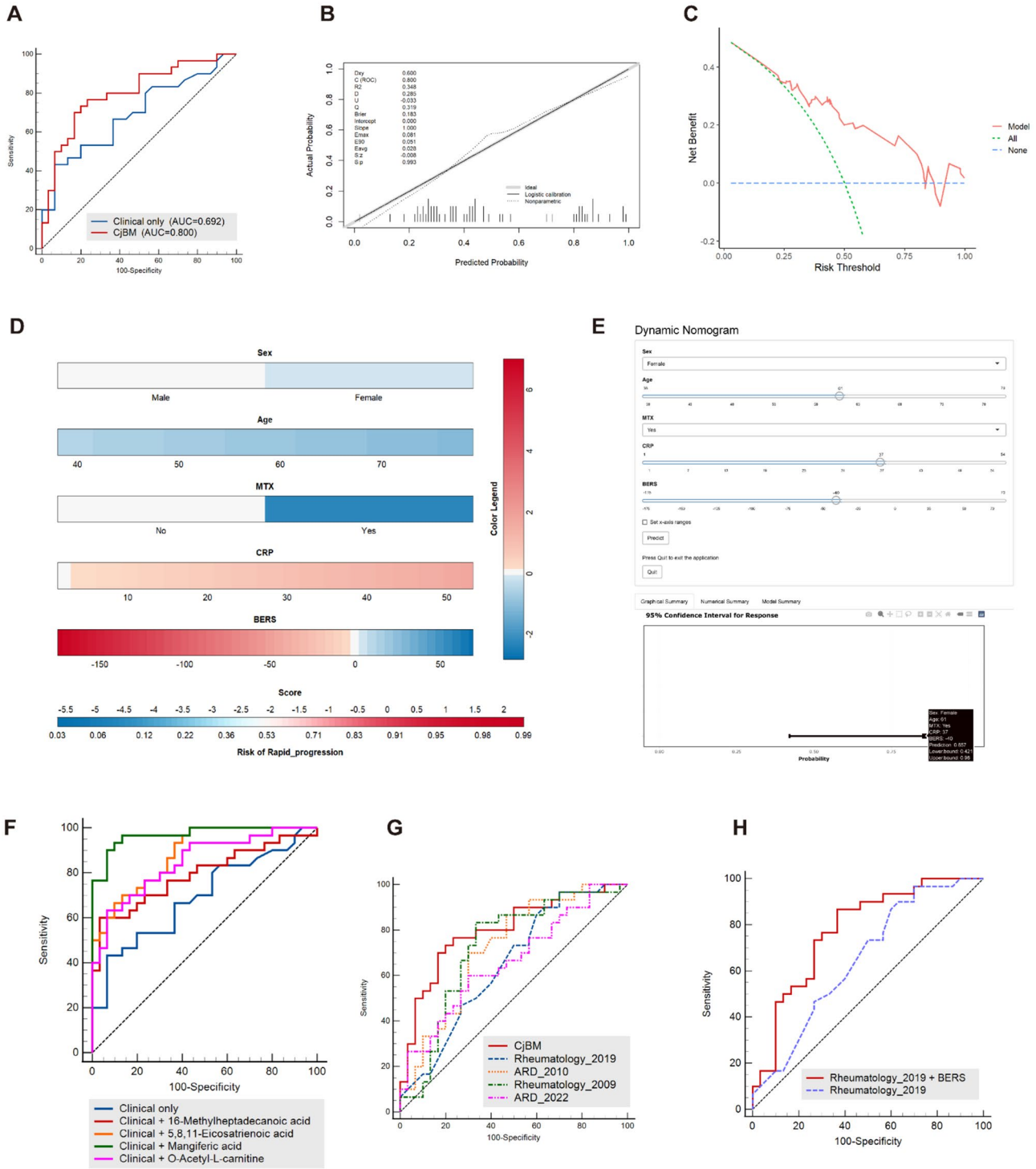

Fig. 5 BERS with integrated clinical indicators predict rapid radiographic progression. (**A**) ROC analysis for predicting rapid radiographic progression in the entire cohort with the LR algorithm model incorporating BERS and clinical indicators. (**B**) A calibration plot for predicting rapid radiographic progression risk using the LR algorithm model across the entire cohort. (**C**) DCA for predicting rapid radiographic progression using the LR algorithm model across the entire cohort. (**D**) The rapid radiographic progression risk scoring model is presented in a colored nomogram. For ease of calculation, BERS is 100-fold of the actual BERS. (**E**) An online rapid radiographic progression risk calculator based on interactive web applications with R/Shiny. For ease of calculation, BERS is 100-fold its actual value. (**F**) ROC analysis for predicting rapid radiographic progression in the entire cohort with the LR algorithm model integrating individual metabolite and clinical indicators. (**G**) ROC analysis for predicting rapid radiographic progression in the entire cohort of the CjBM and previously reported models. (**H**) ROC analysis for predicting rapid radiographic progression in the entire cohort using a previously reported model and incorporating BERS. Abbreviations: BERS, Bone Erosion Risk Score; AUC, area under the curve; MTX, methotrexate; CRP, C-reactive protein; LR, logistic regression; DCA, decision curve analysis; CjBM, China-Japan Friendship Hospital-BERS Model

to predict outcomes. Adding the BERS index significantly increased the AUC of the 2019 model (0.777 vs. 0.694, P_{DeLong}=0.035), enhancing its differentiation capacity (Fig. 5H).

Discussion

Using baseline data from 60 patients with RA, we compared plasma metabolite profiles in patients with different rates of bone destruction progression one year after treatment. Of the 774 identified metabolites, 77 exhibited differences. Four core metabolites were selected using various ML algorithms and ranked by importance. These metabolites showed significantly reduced concentrations in patients with rapid radiographic progression, suggesting their potential to predict the risk of rapid radiographic progression in patients with RA. The findings revealed a significant association between certain plasma metabolites and the risk of rapid radiographic progression in those patients. Furthermore, clinical models incorporating features of plasma metabolites were highly effective in predicting the likelihood of adverse outcomes, including bone erosion and joint functional impairment.

Mangiferic acid was detected at lower levels in patients with rapid radiographic progression, making it the most relevant marker for clinically evaluating the progression of bone destruction in this study. Mangiferic acid, a natural organic polyphenol, is the major metabolite of mangiferin. It is known for its antioxidative and anti-inflammatory properties [26]. Mangiferic acid and mangiferin, often detected in herbal medicines [27], inhibits angiogenesis in synovial tissue [28]. Recent studies found that mangiferin promotes apoptosis of synovial fibroblast cells, blocks the NF-κB signaling pathway, and reduces the levels of matrix metalloproteinases [29, 30], demonstrating therapeutic potential for RA-induced bone destruction. Our analysis showed that using mangiferic acid alone as a predictor can lead to better efficiency for the model. However, to ensure higher external validity and avoid potential false positive results, we used a composite score of four metabolites as the prediction indicator.

O-Acetyl-L-carnitine, an amino acid derivative, is a metabolic product of L-carnitine combined with acetyl and exhibits neuroprotective effects [31]. Within the mitochondria, it promotes fatty acid oxidation and energy production, regulating cellular energy metabolism and oxidative stress response [32]. Currently, clinical studies have found that oral O-acetyl-L-carnitine can improve peripheral neuropathy associated with RA [33], however, no evidence suggests that it has a direct therapeutic effect on RA. The in-vivo experiments suggest that O-acetyl-L-carnitine can target the NF-κB pathway, autophagy, and oxidative stress, thereby alleviating neuroinflammation induced by lipopolysaccharide [34]. This finding facilitates the linkage between the metabolites and inflammation associated with RA. Our findings suggest that O-acetyl-L-carnitine levels can predict bone destruction in RA, which has not been previously reported. Further thorough associations need to be confirmed.

5,8,11-Eicosatrienoic acid, known as mead acid, is an omega-9 polyunsaturated fatty acid with potential antioxidant and protective effects on cell membrane integrity, along with anti-inflammatory properties [35]. This fatty acid is endogenously synthesized and converted into various lipid mediators, which participate in the development of inflammation-related diseases and cancer [36]. Moreover, it can reduce neutrophil infiltration, inhibit MAPK pathway phosphorylation, and suppress the secretion of chemokines in contact dermatitis [37]. However, there is insufficient data to directly support the application of 5,8,11-eicosatrienoic acid in RA treatment. Considering its potential regulatory effect on inflammation and the significance of fatty acid metabolism in RA pathology [38], our findings suggest that 5,8,11-eicosatrienoic acid and its derivatives might be candidate molecules for RA treatment.

16-Methylheptadecanoic acid, a branched saturated fatty acid, has been proposed in oncology research to exhibit antioxidant effects, potentially inhibiting reactive oxygen species-dependent cell apoptosis, positioning it as a target for drug development [39]. Currently, no research has linked 16-methylheptadecanoic acid to rheumatic and immunological diseases. Our results suggest that it plays a potential important role in the progression of RA.

Recently, four high-quality models for predicting bone destruction in patients with RA have been reported. Our comparison of these models, using ROC analysis, revealed that the newly established model "CjBM" exhibits comparable efficacy. The existing models typically incorporate various clinically common features, such as autoantibody, CRP, and ESR levels, as well as the use of antirheumatic drugs, disease activity scores, and imaging scores. The CjBM specifically integrates MTX use and CRP levels, which aligns with the current understanding of RA prognosis [40]. Being the most classic csDMARD, MTX can reduce the risk of bone destruction by regulating the RANKL/RANK/OPG signal transduction pathway and exerting a protective effect on bones and cartilage [41]. Meanwhile, CRP is an indicator used to assess the activity of RA. Low CRP levels are associated with a lower incidence of bone destruction [42], whereas higher levels of CRP are associated with a higher probability of developing complications such as cardiovascular or interstitial lung diseases [43, 44]. We calculated a new BERS by incorporating metabolite features. We stress the highly effective nature of BERS in predicting clinical

results related to bone destruction, and a strong negative nonlinear correlation is demonstrated between BERS and poorer outcomes. The CjBM established based on the BERS index can identify RA adverse outcomes. The AUC of the CjBM reached 0.800, which is satisfactory. Furthermore, we compared CjBM model results with those of the matrix risk model previously reported for identifying rapid radiographic progression in RA [7]. After incorporating the BERS index, we observed a certain enhancement in the efficacy of the radiographic progression prediction. These findings emphasize the potential of plasma metabolites in categorizing high-risk populations and indicate that metabolite features can serve as a feasible method for predicting bone destruction in RA, laying the groundwork for active interventions to mitigate the risk of bone destruction progression in the future.

Our study presents several advantages. By integrating metabolomics with commonly used clinical indicators, we could identify and analyze hundreds of metabolites in the peripheral blood plasma in patients with RA. Second, 60 patients were followed for one year, allowing us to track the changes in the clinical outcomes of bone destruction over an extended period. During feature analysis and model establishment, several ML algorithms were employed. These algorithms can explain the association between metabolites and clinical outcomes more efficiently and rationally, leading to highly stable results. Additionally, we developed a new index "BERS" integrating overall metabolite features with the clinical outcomes. This index detected a relationship between metabolites and bone destruction-related outcomes, an association previously unreported.

Some issues need to be addressed before the results can be generalized. Although the training, validation, and test sets were partitioned during analysis to guarantee the stability of the results, the small sample size of 60 cases may lead to overfitting. Increasing the cohort size, as well as incorporating an external test set, would be beneficial. While our metabolomics analysis identified 77 differentially expressed metabolites and highlighted four core biomarkers, the mechanistic relationships between these metabolites and RA-induced bone erosion remain to be fully elucidated. Further experimental studies are needed to establish potential causal links.

Conclusions

We proposed the BERS index, derived from plasma metabolite features, which can be applied clinically to stratify the risk of bone erosion. We have established a prediction model "CjBM" for assessing the risk of bone destruction in patients with RA based on clinical indicators and plasma metabolite features. The CjBM has certain advantages over previously published models. These results promote our understanding of RA-related bone destruction. The metabolite-based prediction model powered by ML algorithms provides valuable guidance for dynamic monitoring and targeted management of RA.

Abbreviations

ACPA	Anticyclic citrullinated polypeptide antibody
AdBoost	Adaptive boosting
AUC	Area under the curve
BERS	Bone Erosion Risk Score
BMI	Body mass index
CI	confidence interval
CjBM	China-Japan Friendship Hospital-BERS Model
CRP	C-reactive protein
CsDMARDs	Conventional synthetic disease-modifying antirheumatic drugs
DAS28	Disease activity score derivative for 28 joints
DCA	Decision curve analysis
ESR	Erythrocyte sedimentation rate
ESS	Erosion Sharp score
GBDT	Gradient Boosting Decision Tree
GNB	Gaussian Naive Bayes
HAQ-DI	Health Assessment Questionnaire-Disability Index
HMDB	Human Metabolome Database
IQR	Interquartile range
KEGG	Kyoto Encyclopedia of Genes and Genomes
LASSO	Least absolute shrinkage and selection operator
LC-MS	Liquid chromatograph-mass spectrometer
LightGBM	Light Gradient Boosting Machine
LR	Logistic regression
ML	Machine learning
MLP	Multilayer Perceptron
MMPs	Matrix metalloproteinases
Mtss	Van der Heijde-modified total Sharp score
MTX	Methotrexate
NRI	Net reclassification improvement
NSS	Narrowing Sharp score
OR	Odds ratios
PCA	Partial least squares discriminant analysis
RA	Rheumatoid arthritis
RCS	Restricted cubic spline
RCT	Randomized controlled trial
RF	Rheumatoid factor
ROC	Receiver operating characteristic
SD	Standard deviation
SHAP	SHapley Additive exPlanations
SJC28	Swollen joint count for 28 joints
SVM	Support vector Machine
TJC28	Tender joint counts for 28 joints
VAS	Visual analogue scale
XGBoost	eXtreme Gradient Boosting

Supplementary Information

The online version contains supplementary material available at https://doi.org/10.1186/s13075-025-03576-x.

Supplementary Material 1

Supplementary Material 2

Supplementary Material 3

Supplementary Material 4

Supplementary Material 5

Acknowledgements

The Department of Traditional Chinese Medicine Rheumatism, China-Japan Friendship Hospital provided support with data collection and interpretation.

Author contributions
Conceptualization, Cheng Xiao, Qingwen Tao and Yuan Xu; Methodology, Hongwei Yu and Jiahe Xu; Software, Qishun Geng; Validation, Xing Wang and Yi Jiao; Writing – Original Draft Preparation, Zihan Wang and Tianyi Lan. All authors commented on previous versions of the manuscript. All authors read and approved of the final manuscript.

Funding
This work was supported by National High Level Hospital Clinical Research Funding [grant number 2022-NHLHCRF-LX-02-02] and National Natural Science Foundation [grant number 82474275].

Data availability
Some, not all, original data may be shown upon request to a limited extent. However, some other data cannot be obtained due to the confidentiality of the patients' personal information.

Declarations

Ethics approval and consent to participate
This study was approved by the China-Japan Friendship Hospital Clinical Research Ethics Committee (2020-133-K86). The study was conducted in accordance with the Declaration of Helsinki. Each patient provided informed consent at the time of investigation to allow the use of their clinical records for further scientific reporting.

Consent for publication
Written informed consent was obtained from the patients for publication of the research. A copy of the written consent is available for review by the Editor-in-Chief of this journal.

Competing interests
The authors declare no competing interests.

Author details
[1]Department of Traditional Chinese Medicine Rheumatism, China-Japan Friendship Hospital, No. 2 Yinghua East Street, Chaoyang District, Beijing, People's Republic of China
[2]Graduate School, Beijing University of Chinese Medicine, Beijing, People's Republic of China
[3]Department of Radiology, China-Japan Friendship Hospital, Beijing, People's Republic of China
[4]China-Japan Friendship Clinical Medical College, Chinese Academy of Medical Sciences & Peking Union Medical College, Beijing, People's Republic of China
[5]Peking University China-Japan Friendship School of Clinical Medicine, Beijing, People's Republic of China
[6]Institute of Clinical Medicine, China-Japan Friendship Hospital, No. 2 Yinghua East Street, Chaoyang District, Beijing, People's Republic of China

Received: 20 January 2025 / Accepted: 13 May 2025
Published online: 21 May 2025

References

1. Di Matteo A, Bathon JM, Emery P. Rheumatoid arthritis. Lancet. 2023;402(10416):2019–33.
2. Sparks JA, Harrold LR, Simon TA, Wittstock K, Kelly S, Lozenski K, et al. Comparative effectiveness of treatments for rheumatoid arthritis in clinical practice: A systematic review. Semin Arthritis Rheum. 2023;62:152249.
3. Almutairi K, Nossent J, Preen D, Keen H, Inderjeeth C. The global prevalence of rheumatoid arthritis: a meta-analysis based on a systematic review. Rheumatol Int. 2021;41(5):863–77.
4. Komatsu N, Takayanagi H. Mechanisms of joint destruction in rheumatoid arthritis - immune cell-fibroblast-bone interactions. Nat Rev Rheumatol. 2022;18(7):415–29.
5. Aletaha D. Precision medicine and management of rheumatoid arthritis. J Autoimmun. 2020;110:102405.
6. Orsini F, Crotti C, Cincinelli G, Di Taranto R, Amati A, Ferrito M, et al. Bone involvement in rheumatoid arthritis and spondyloartritis: an updated review. Biology (Basel). 2023;12(10):1320.
7. Vastesaeger N, Xu S, Aletaha D, St Clair EW, Smolen JS. A pilot risk model for the prediction of rapid radiographic progression in rheumatoid arthritis. Rheumatology (Oxford). 2009;48(9):1114–21.
8. Adami G, Fassio A, Pistillo F, Benini C, Viapiana O, Rossini M, et al. Factors associated with radiographic progression in rheumatoid arthritis starting biological diseases modifying anti-rheumatic drugs (bDMARDs). Ther Adv Musculoskelet Dis. 2023;15:1759720x231174534.
9. Visser K, Goekoop-Ruiterman YP, de Vries-Bouwstra JK, Ronday HK, Seys PE, Kerstens PJ, et al. A matrix risk model for the prediction of rapid radiographic progression in patients with rheumatoid arthritis receiving different dynamic treatment strategies: post hoc analyses from the best study. Ann Rheum Dis. 2010;69(7):1333–7.
10. Vanier A, Smolen JS, Allaart CF, Van Vollenhoven R, Verschueren P, Vastesaeger N, et al. An updated matrix to predict rapid radiographic progression of early rheumatoid arthritis patients: pooled analyses from several databases. Rheumatology (Oxford). 2020;59(8):1842–52.
11. Cedeno M, Murillo-Saich J, Coras R, Cedola F, Brandy A, Prior A, et al. Serum metabolomic profiling identifies potential biomarkers in arthritis in older adults: an exploratory study. Metabolomics. 2023;19(4):37.
12. Moulin D, Millard M, Taïeb M, Michaudel C, Aucouturier A, Lefèvre A, et al. Counteracting Tryptophan metabolism alterations as a new therapeutic strategy for rheumatoid arthritis. Ann Rheum Dis. 2024;83(3):312–23.
13. Dudka I, Chachaj A, Sebastian A, Tański W, Stenlund H, Gröbner G, et al. Metabolomic profiling reveals plasma glyca and GlycB as a potential biomarkers for treatment efficiency in rheumatoid arthritis. J Pharm Biomed Anal. 2021;197:113971.
14. Fang XY, Zhang J, Qian TT, Gao P, Wu Q, Fang Q, et al. Metabolomic profiles, polygenic risk scores and risk of rheumatoid arthritis: a population-based cohort study in the UK biobank. RMD Open. 2023;9(4):e003560.
15. Koh JH, Yoon SJ, Kim M, Cho S, Lim J, Park Y, et al. Lipidome profile predictive of disease evolution and activity in rheumatoid arthritis. Exp Mol Med. 2022;54(2):143–55.
16. Lan T, Wang Z, Yan Z, Yao C, Yu H, Ma E, et al. The delaying effect of Bushen Zhiwang Decoction on bone destruction in rheumatoid arthritis patients with a pattern of deficiency of both liver and kidney based on modified total Sharp score. J Beijing Univ Trad Chin Med. 2023;46(4):557–63.
17. Aletaha D, Neogi T, Silman AJ, Funovits J, Felson DT, Bingham CO 3rd, et al. 2010 Rheumatoid arthritis classification criteria: an American college of rheumatology/european league against rheumatism collaborative initiative. Ann Rheum Dis. 2010;69(9):1580–8.
18. van der Heijde DM. Plain X-rays in rheumatoid arthritis: overview of scoring methods, their reliability and applicability. Baillieres Clin Rheumatol. 1996;10(3):435–53.
19. Koo BS, Eun S, Shin K, Hong S, Kim YG, Lee CK, et al. Differences in trajectory of disease activity according to biologic and targeted synthetic disease-modifying anti-rheumatic drug treatment in patients with rheumatoid arthritis. Arthritis Res Ther. 2022;24(1):233.
20. DeLong ER, DeLong DM, Clarke-Pearson DL. Comparing the areas under two or more correlated receiver operating characteristic curves: a nonparametric approach. Biometrics. 1988;44(3):837–45.
21. Durrleman S, Simon R. Flexible regression models with cubic splines. Stat Med. 1989;8(5):551–61.
22. Zou L, Choi YH, Guizzetti L, Shu D, Zou J, Zou G. Extending the DeLong algorithm for comparing areas under correlated receiver operating characteristic curves with missing data. Stat Med. 2024;43(21):4148–62.
23. Jewell ES, Maile MD, Engoren M, Elliott M. Net Reclassification Improv Anesth Analg. 2016;122(3):818–24.
24. Jia L, Yao W, Jiang Y, Li Y, Wang Z, Li H, et al. Development of interactive biological web applications with R/Shiny. Brief Bioinform. 2022;23(1):bbab415.
25. Platzer A, Alasti F, Smolen JS, Aletaha D, Radner H, Blüml S. Trajectory clusters of radiographic progression in patients with rheumatoid arthritis: associations with clinical variables. Ann Rheum Dis. 2022;81(2):175–83.
26. Mei S, Perumal M, Battino M, Kitts DD, Xiao J, Ma H, et al. Mangiferin: a review of dietary sources, absorption, metabolism, bioavailability, and safety. Crit Rev Food Sci Nutr. 2023;63(18):3046–64.
27. Mao X, Liu Y, Li W, Wang K, Li C, Wang Q, et al. A promising drug combination of mangiferin and glycyrrhizic acid ameliorates disease severity of rheumatoid arthritis by reversing the disturbance of thermogenesis and energy metabolism. Phytomedicine. 2022;104:154216.

28. Mao X, Yan X, Li C, Liu Y, Zhang Y, Lin N. Extensive preclinical evaluation of combined mangiferin and glycyrrhizic acid for restricting synovial neovascularization in rheumatoid arthritis. Chin Med. 2023;18(1):156.
29. Akkewar AS, Mishra KA, Sethi KK, Mangiferin. A natural bioactive Immunomodulating glucosylxanthone with potential against cancer and rheumatoid arthritis. J Biochem Mol Toxicol. 2024;38(7):e23765.
30. Wang R, Liu J, Wang Z, Wu X, Guo H, Jiao X, et al. Mangiferin exert protective effects on joints of adjuvant-induced arthritis rats by regulating the MAPKs/NF-κB pathway of fibroblast-like synoviocytes. Int Immunopharmacol. 2021;101(Pt B):108352.
31. Alhusaini A, Sarawi W, Mattar D, Abo-Hamad A, Almogren R, Alhumaidan S, et al. Acetyl-L-carnitine and/or liposomal co-enzyme Q10 prevent propionic acid-induced neurotoxicity by modulating oxidative tissue injury, inflammation, and ALDH1A1-RA-RARα signaling in rats. Biomed Pharmacother. 2022;153:113360.
32. Izzo LT, Trefely S, Demetriadou C, Drummond JM, Mizukami T, Kuprasertkul N, et al. Acetylcarnitine shuttling links mitochondrial metabolism to histone acetylation and lipogenesis. Sci Adv. 2023;9(18):eadf0115.
33. Parisi S, Ditto MC, Borrelli R, Fusaro E. Efficacy of a fixed combination of palmitoylethanolamide and acetyl-l-carnitine (PEA + ALC FC) in the treatment of neuropathies secondary to rheumatic diseases. Minerva Med. 2021;112(4):492–9.
34. Jamali-Raeufy N, Alizadeh F, Mehrabi Z, Mehrabi S, Goudarzi M. Acetyl-L-carnitine confers neuroprotection against lipopolysaccharide (LPS) -induced neuroinflammation by targeting TLR4/NFκB, autophagy, inflammation and oxidative stress. Metab Brain Dis. 2021;36(6):1391–401.
35. Kawashima H, Yoshizawa K. The physiological and pathological properties of Mead acid, an endogenous multifunctional n-9 polyunsaturated fatty acid. Lipids Health Dis. 2023;22(1):172.
36. Farag MA, Gad MZ. Omega-9 fatty acids: potential roles in inflammation and cancer management. J Genet Eng Biotechnol. 2022;20(1):48.
37. Saika A, Tiwari P, Nagatake T, Node E, Hosomi K, Honda T, et al. Mead acid inhibits retinol-induced irritant contact dermatitis via peroxisome proliferator-activated receptor alpha. Front Mol Biosci. 2023;10:1097955.
38. Kraus FV, Keck S, Klika KD, Graf J, Carvalho RA, Lorenz HM, et al. Reduction of Proinflammatory effector functions through remodeling of fatty acid metabolism in CD8 + T cells from rheumatoid arthritis patients. Arthritis Rheumatol. 2023;75(7):1098–109.
39. Saravanakumar K, Vivek R, Sithranga Boopathy N, Yaqian L, Kathiresan K, Chen J. Anticancer potential of bioactive 16-methylheptadecanoic acid Methyl ester derived from marine Trichoderma. J Appl Biomed. 2015;13(3):199–212.
40. Brown P, Pratt AG, Hyrich KL. Therapeutic advances in rheumatoid arthritis. BMJ. 2024;384:e070856.
41. Destiani DP, Naja S, Dewi S, Rahmadi AR, Sulaiman SAS, Abdulah R. Efficacy of methotrexate in reducing the risk of bone erosion in patients with rheumatoid arthritis: a systematic review of randomized controlled trials. Osteoporos Int. 2021;32(5):805–16.
42. Liang C, Li J, Lu C, Xie D, Liu J, Zhong C, et al. HIF1α Inhibition facilitates Leflunomide-AHR-CRP signaling to attenuate bone erosion in CRP-aberrant rheumatoid arthritis. Nat Commun. 2019;10(1):4579.
43. Zhang M, Yin J, Zhang X. Factors associated with interstitial lung disease in patients with rheumatoid arthritis: A systematic review and meta-analysis. PLoS ONE. 2023;18(6):e0286191.
44. Erre GL, Cacciapaglia F, Sakellariou G, Manfredi A, Bartoloni E, Viapiana O, et al. C-reactive protein and 10-year cardiovascular risk in rheumatoid arthritis. Eur J Intern Med. 2022;104:49–54.

Publisher's note